IOP Conference Series: Materials Science and Engineering

PAPER • OPEN ACCESS

Micro-Indentation of oxidized low carbon steel to evaluate properties of oxides

To cite this article: V Claverie-Burgué *et al* 2022 *IOP Conf. Ser.: Mater. Sci. Eng.* **1270** 012106

IOP Conf. Series: Materials Science and Engineering 1270 (2022) 012106 doi:10.1088/1757-899X/1270/1/012106

Micro-Indentation of oxidized low carbon steel to evaluate properties of oxides

V Claverie-Burgué[1,2], P Montmitonnet[1], K Inal[1], A Burr[1], A Nicolaÿ[1], M Picard[2] and A Settefrati[2]
[1] MINES Paris, PSL Research University, Centre de mise en forme des matériaux (CEMEF), CNRS [UMR 7635], 06904 Sophia Antipolis Cedex, France
[2] ArcelorMittal Maizières Research SA, Voie Romaine, 57280 Maizières-lès-Metz, France

Abstract. During hot rolling process, an oxide scale grows at the surface of steel slabs. To avoid surface defects such as embedded scale at the end of the finishing mill, descaling stands are added in the production line to remove it using high-pressure water jets. Different steel grades show different descaling capacities and final surface qualities, which may depend on composition through oxide and interface toughness. The idea of this study is to measure the latter using micro-indentation to feed thermomechanical models of the descaling process. After indentation, Focused Ion Beam (FIB) is employed to observe cracking and delamination of oxidized specimen and to calculate adhesion of oxide thanks to an analytical formula. The experimental study confirms that alloying elements have a strong influence on the adhesion of oxide film and suggests that difficult-to-descale grades are those showing a large scatter of interfacial toughness. In parallel, numerical finite element (FEM) simulations of indentation are carried out using Abaqus® to have a better understanding of cracking mechanism and delamination of oxide.

1. Introduction

During the hot rolling process, steel slabs are heated at high temperature (1200°C) to be made softer (reduction of the roll load), more deformable and to transform the improper casting microstructure. At high temperature, an oxide scale is produced on the surface of the slabs. For low carbon steel, it consists of three components: Wustite $Fe_{1-x}O$ (~90%) in contact with the steel, an intermediate layer of Magnetite Fe_3O_4 (~8%) and a thin layer at the surface (~2%) of Hematite Fe_2O_3. The percentage is given as an average indication but of course may vary depending on grades and the rolling parameters (speed, temperature…). Unfortunately, this thick scale (~100 µm at the entry of the finishing mill) induces some surface defects during rolling and it has to be removed. Some descaling stands are therefore added in the production line to remove it and to improve the surface quality of the final product. By sending 150 bar-pressurized water on the scale, mechanical and thermal stresses make the oxide layer crack and spall.
The work reported here is a part of an on-going study, which consists in designing and carrying out experiments at high temperature to understand the oxide scale behaviour during descaling. This includes characterization of both oxide and steel and their interface, which is essential to determine a stress-based fracture criterion relevant for the computation of descaling. Moreover at high temperature, oxide scale undergoes a ductile-brittle transition which has been reported in literature during hot rolling [1–4]. It is essential to identify this transition and measure oxide and interface properties below and above the transition temperature to optimize descaling process.
Scratch testing is the standard way of estimating qualitatively the adhesion of coatings. Some attempts at high temperature scratch testing have been reported [5–9] but on the one hand they are complex to carry out and on the other hand, it is difficult to extract reliable quantitative toughness parameters.

Therefore, the project final aim is to implement a hot indentation test. Indentation is adapted to solicit oxide and its interface to active delamination mechanism, the one that is essential in descaling. Several models have been developed to evaluate adhesion of thin film on a substrate [10–16]. Recently, indentation tests at high temperature have been successfully carried out, overcoming technical difficulties (thermal drift, degradation of diamond indenter…) [17–20].
In the present paper, Room Temperature (RT) indentation of pre-oxidized samples is carried out as a first step, to demonstrate the capability of the approach which combines:

- indentation tests at different loads (i.e. indentation depth/oxide thickness ratios),
- FIB cutting on indentation marks to investigate the diverse types of cracks, in particular to measure interfacial crack length,
- Apply theoretical models to evaluate interfacial toughness from interfacial crack length. Both an analytical formula and FEM modelling with ABAQUS® are used for this purpose.

2. Experimental procedure

2.1. Controlled oxidation of low carbon steel
Three grades are selected for this study: Interstitial Free steel (IF), High Strength steel (HS) and a third grade called here N1. The last two are difficult to descale in production. In Table 1, percentages of C and Mn of each grade are presented (other elements are similar between them). Specimens have been manually polished with a SiC abrasive paper (granulometry 22 µm) and oxidized in a controlled atmosphere furnace at 650°C or 700°C. Different oxidation times and percentages of oxygen are selected to vary the thickness of oxide in the range 15 – 60 µm. For example, oxidation at 650°C for 410 s with air (20.9% of oxygen) forms a 26µm oxide thickness.

Table 1 . Compositions of the 3 grades.

Grades	C%	Mn%
HS	0.078	0.435
IF	<0.002	0.088
N1	0.117	0.558

2.2. Indentation at room temperature
A homemade apparatus intended for high temperature instrumented indentation is used, here at RT, in the 2 - 45N load range. A standard micro-indentation tester (Buehler) is also used from 0.05 to 5N. In both cases, RT indentations on pre-oxidized specimens are made using a Diamond Vickers indenter. Indentation tests are performed in 3 steps. First, a loading step to the desired force at an indention speed of 3 µm/s is realized. The load is then maintained for 10s before the final unloading (same speed than the loading step).

2.3. Observations of indentation with SEM and FIB
After indentation, multiple fractures are observed on the oxide surface, as observed using a Scanning Electron Microscopy (SEM, MAIA3, Tescan, see Fig. 1). In order to have information at the interface between steel and oxide, cross-sections are prepared using a plasma (Xe source) Focus Ion Beam (FIB) thanks to a FIB column mounted on a SEM (Tescan FERA3 dual beam microscope). Cross-sections are obtained in 3 milling steps. Cross-sections opening is performed at 30 kV and high current (2 µA). The resulting cross-section is then polished at 30 kV and a current intensity of 1 µA. Finally, the FIB current intensity is reduced down to 100 nA to refine the cross-section surface quality.

3. Results

3.1. Fracture mechanism due to indentation

In order to facilitate comparison between specimens of different thickness, a normalisation is done by dividing the penetration of indenter p by the oxide thickness t (p/t). Once indentation has been carried out, surface observations highlight "circular" cracks (Figure 1). All along the loading, more cracks appear periodically. For a given grade, and for a constant thickness, the critical force for the first superficial crack is 1N for the IF grade and it corresponds to p/t=0.1. As a reminder, when ratio p/t > 0.1, results are more and more strongly influenced by the substrate. It indicates that fracture behaviour of oxide depends on substrate: for low force indentation, oxide is not fractured, as long as the substrate does not yield; when it does, it forces the whole oxide layer to bend under the indenter. With increasing load, the bending effect increases and other cracks form. Starting from the corners of indentation, radial cracks are observed as well.

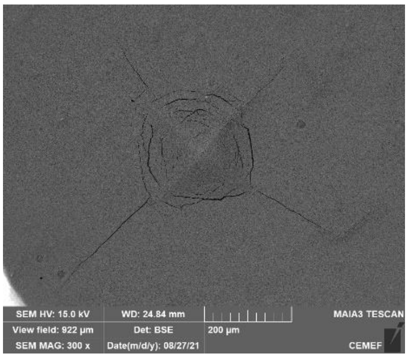

Figure 1. SEM observation of oxidized specimen (26µm) after a 40N indentation

(a) (b)

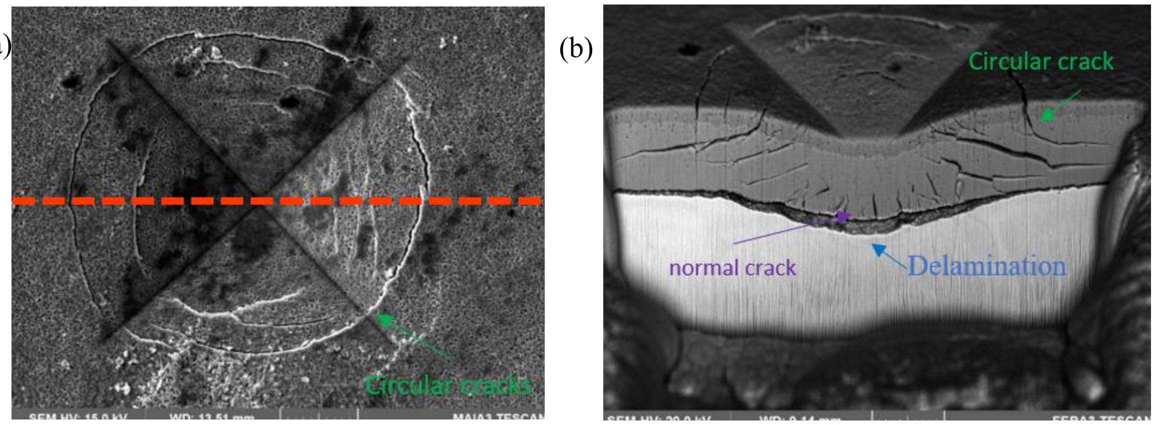

Figure 2. SEM observation of oxidized IF specimen indentation with 5N force (p/t~0.6). (a) top view showing circular cracks. (b) cross-section of the indentation, the cross-section is prepared by milling the imprint along the red-line, perpendicular to the top surface.

However, by optical observation from the surface, information is missing, particularly what is happening at the interface between oxide and steel. A cross-section is prepared by milling the vicinity of the indentation with FIB technology (Figure 2b and Figure 3b). These cross-sectional observations bring an important complement of information:

1) in reality, circular cracks deviate outwards and do not propagate to the interface with steel
2) radial cracks propagate to the interface
3) delamination is observed below indentation. This indicates a poor adhesion of oxide on this steel grade under these conditions. This delamination is commonly described in literature [10,11]. The

large compression zone below the indenter makes thin film buckle (if a compression threshold is reached).

4) normal cracks starting perpendicular to the interface are also present. This is due to the oxide layer bending following plastic deformation of steel; fracture occurs on the extrados.

These crack mechanisms at room temperature are reproducible for all these three grades (IF, HS and N1). Some regions far from indentations are also milled, showing that initially, the oxide is perfectly bonded, with no interfacial gap (Figure 4).

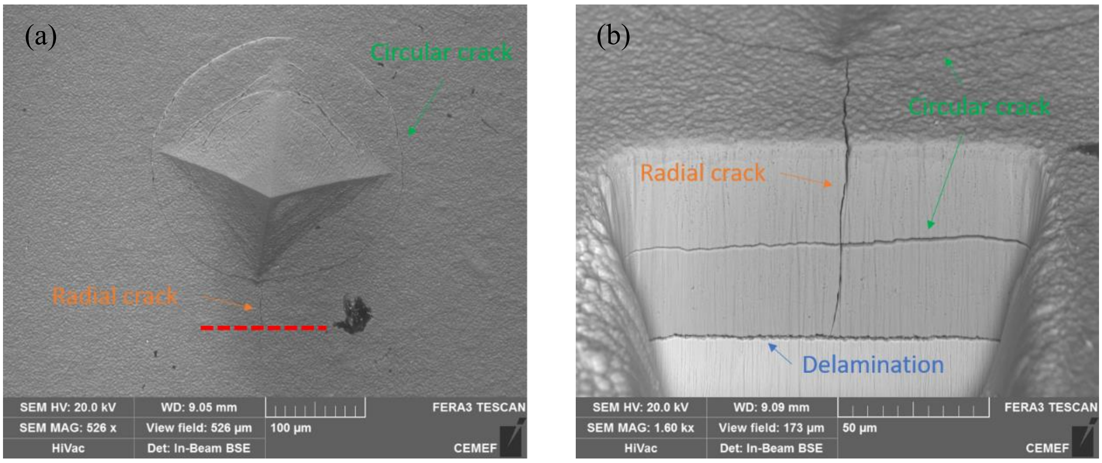

Figure 3 . SEM observation of oxidized IF specimen indentation with 30N force (55µm of thickness). (a) top view showing circular and radial cracks. (b) cross-section of the indentation, the cross-section is prepared by milling the impression along the red-line, perpendicular to the top surface.

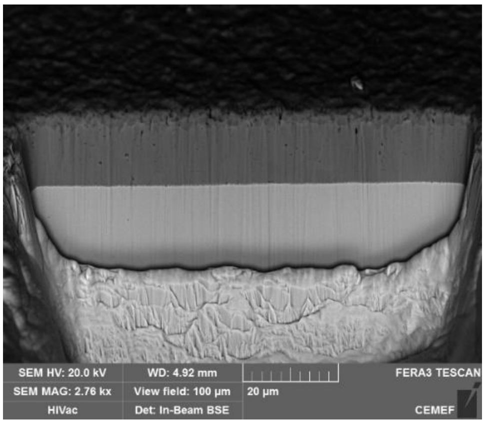

Figure 4. cross-section observation of oxidized specimen in an area without indentation (IF grade).

3.2. Evaluation of adhesion value: G_c interfacial adhesion energy

Propagation of fracture at the interface between oxide and steel is representative of adherence of scale. Adhesion of a thin film is controlled by interfacial bonding strength. Indeed, indentation can be used to stress the interface and generate delamination. G, the energy release rate, is the drop of strain energy in the system brought about by a unit increase of crack surface area. It is related to the stress intensity factor K (proportional to the load) by $G = K^2/E$. G provides the energy needed to create new surface (surface energy γ), plus some inelastic strain energy if needed to propagate the crack (plasticity or viscoelasticity at crack tip). In case of non-dissipative, elastic behaviour, equilibrium propagation implies that $G = 2\gamma$. Therefore, following crack propagation provides a quantitative determination of interface energy. Rosenfeld [12] determines interfacial fracture energy of epoxy coating on soda-lime glass substrate by considering that debond crack is driven by contact stresses during loading. This model is efficient when the delaminated area is an annulus of inner radius a, the contact radius, and outer radius c (crack extension). The interfacial adhesion energy G is given by:

$$G = \frac{2(1-\nu_c^2)\sigma_{rb}{}^2 h_c}{E_c}\left[1-\nu_c+(1-\nu_c)\left(\frac{c}{a}\right)^2\right]^{-2} \tag{1}$$

E_c and ν_c are the Young's modulus and Poisson's ratio of the coating, h_c its thickness. σ_{rb} is the radial stress at the outer edge of the contact zone at full load; it is calculated by applying the Tresca yield criterion to the plastically deformed zone contact. They assumed that $\sigma_{rb} = \sigma_{yc} - H_c$ where σ_{yc} is the yield stress and H_c is the hardness of the coating and an approximation of the hydrostatic stress. The H_c/σ_{yc} ratio is approximately 3. This method is also used to evaluate properties of a Diamond-like carbon (DLC) thin film on a steel substrate [21].
The exploitation of this analytical model is based on debond crack size measurements. Only specimens on which delamination is observed are considered. For IF grade, Figure 5 represents calculated G_c value as a function of thickness (a) and ratio p/t (b). G_c seems to be reasonably independent of thickness and p/t. However, for this grade, when ratio p/t is lower than 0.1, no delamination is observed. In this case, influence of steel substrate is very limited. Yet, for a same sample (16 µm), dispersion is present and suggests heterogeneity of the metal-oxide interface, although the preparation method and the indentation itself may bring part of the variance.

(a)

(b)

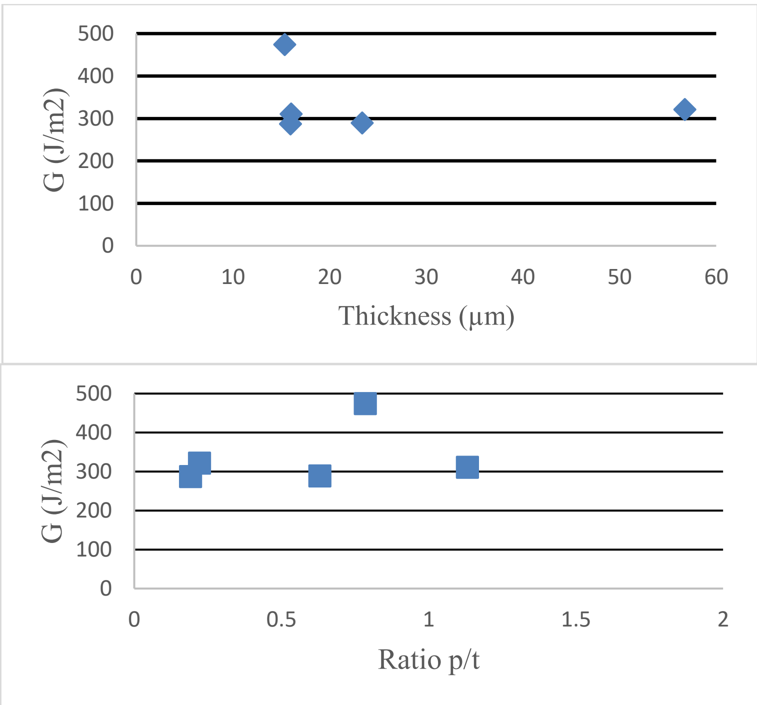

Figure 5. Influence of thickness (a) and ratio p/t (b) on G_c for IF grade.

For HS and N1, indentations are carried out from 0.5 to 20 N. For samples with a thickness higher than 20 µm, oxide has been completely flaked-off during indention. Thus, adhesion values are calculated for samples with thickness lower than 20 µm . Even for low force indentation, delamination of oxide is larger than cross-section lateral size (Figure 6). This reflects poor adhesion of theses grades. Once delamination has started, the fracture is propagated far from indentation area.

(a) (b)

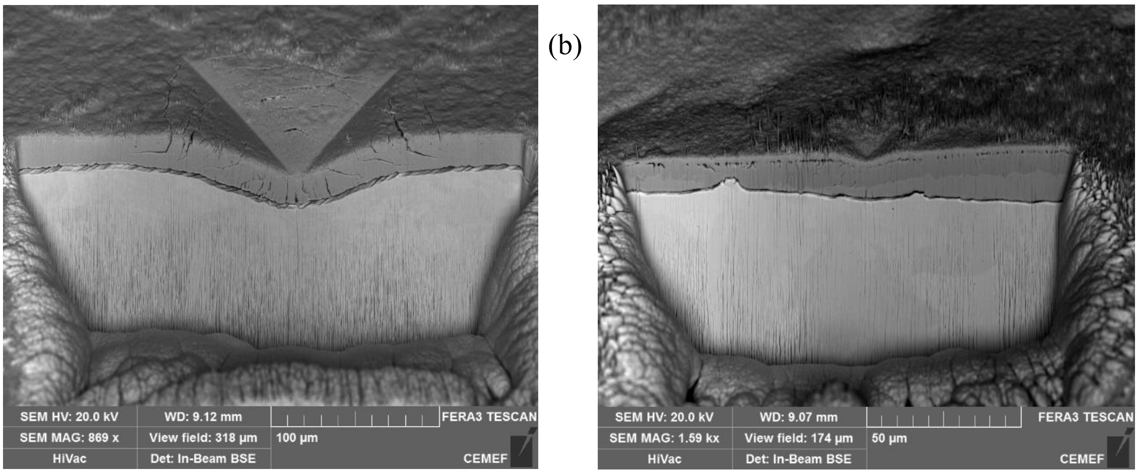

Figure 6. SEM observation of oxidized N1 specimen after indentation (a) with 20N force. (b) with 1N. The cross-section is prepared by milling perpendicular to the top surface. Grey level contrast shows oxide heterogeneity as magnetite appears darker in BSE (Back-Scattered Electron) mode due to higher oxygen content and lower average atomic mass.

Results for three grades are presented in

Table **2**. Adhesion for HS and N1 is much lower than for IF. Standard deviation has the same order of magnitude as the average for HS and N1, it reflects the large heterogeneity of adherence for these grades. This method used to determine adhesion of oxide scale shows a large variability in results. This may be due partly to the uncertainty of the methodology, but also to the spatial variability of the adhesion and, presumably, the interface composition or microstructure. Thus, it is then necessary to multiply the analyses to refine results.

Table 2. Adherence value calculated thanks to indentation method.

Grade	G_c (J/m^2)	
	Average	Min-Max
IF	336 ± 39	287 – 474
HS	45 ± 30	0 – 136
N1	43 ± 33	1 - 139

3.3. Numerical simulation of indentation

Room temperature indentation results show competition between the delamination, of interest to us, and spurious through-thickness cracks which may prevent observation of the former. The combination of simulation and experimental tests is useful to understand the behavior of the material, it is frequently used for indentation test on thin film [22–26].

Indentation simulations are launched in order to understand cracking mechanism in oxide. Simulation is simplified using 2D axis-symmetry, with as usual an indenter angle of 71.3° (Vickers equivalent [27]). The thickness of oxide is 26 µm . After some tests, a computation volume of 250 µm (radius) x 100 µm (thickness) has been found sufficient to avoid edge effects. The same mesh size (0.5 µm) is used in oxide and steel, and 4-node bilinear axisymmetric quadrilateral elements with reduced integration are selected. Both the loading and the unloading are simulated. Reference node is localized at the top of the indenter, a displacement is applied in the -z direction at a speed of 3µm/s. Indenter is considered as a rigid body for simplicity due to its high hardness and modulus. No-displacement boundary conditions are applied to the bottom of the steel part and to the external side of the sample. Interaction between indenter and oxide is specified as master-slave surface (indenter is master) with friction $\mu = 0.1$ (Coulomb model) imposed by a penalty technique and unilateral contact normal behaviour (hard contact and separation allowed after contact).

The behaviours of each materials are considered elasto-visco-plastic. The Young's moduli of the oxide and the steel at room temperature are respectively 240 GPa and 210 GPa [28], both Poisson's coefficients are 0.3. The visco-plastic part follows a Hollomon-type model where K the consistency, the strain hardening exponent n and the strain rate sensitivity coefficient m depend on temperature T:

$$\sigma = K(T).\varepsilon^{n(T)}.\dot{\varepsilon}^{m(T)} \qquad (2)$$

For steel, K value is directly calculated using Tabor formula [29], considering that flow stress is equal to Vickers Hardness divided by three for a representative strain of 0.08. As ratio of hardness between oxide and steel at room temperature is equal to 3 (Hv_{steel} = 1.9 GPa, Hv_{oxide} = 6.5 GPa), the assumption is made that $K_{oxide} = 3\ K_{steel}$. For steel, m is set as 0.01 and n=0.152 in agreement with data calculated by Picqué using 4 point bending tests on low carbon steel [1]. For oxide, a strong assumption is made by which the n and m coefficients are chosen identical to those of steel. All parameters used are indicated in Table 3. Neither compressive residual stresses due to the thermal stresses during cooling nor growth stress are taken into consideration [30].

Table 3. Material parameters used in numerical simulation.

Material law Parameter	Steel	Oxide
K (MPa)	1076	3230
m	0.152	0.152
n	0.01	0.01
E (GPa)	210	240
Poisson's coefficient	0.3	0.3

It is useful to observe stress field to predict zone where failure may happen (Figure 7). In surface, the 11 (radial: Figure 7(a)) and 33 (circumferential: Figure 7(c)) stress components are in tension near the contact edge, and are increasing all along the loading. At the end of the loading, maximums are reached (respectively 1700 and 1000 MPa). In experimental indentation tests, first circular and then radial cracks appear at the surface. This highly bi-component stress area confirms localization of cracks in surface. Experimental work shows that these circular cracks are not propagated until interface. From a certain stage of oxide bending, a compression area is present at the interface (11-stress component), below the edge of indentation. This bending field (surface in tension and compression at the interface) channels crack outward more and more horizontally. The 33-stress component is in tension all along oxide, it allows propagation of radial crack to the interface and outwards, since the oxide is in tension all through the thickness and to a radius at least twice the indentation radius. At the interface, values of normal stress are largely compressive (Figure 7(b)). The shearing component (Figure 7(d)) is larger below indentation contact edge. It is seen that delamination is likely to initiate where this component is maximal (400 MPa), and delamination behaviour remains in mode II. Once oxide is delaminated, interface is bent which leads to normal cracks starting from the interface. During unloading, due to the visco-plastic behaviour, all stresses are relaxed in the long run, we have found no stress component suggesting crack initiation.

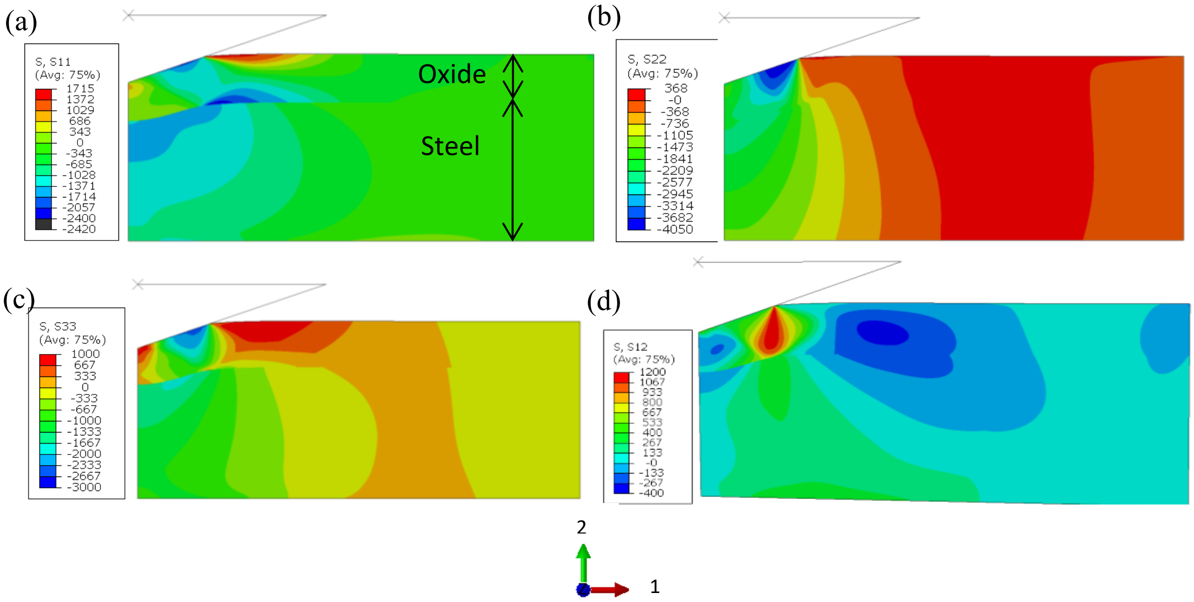

Figure 7. Stress distribution: (a) 11 component, (b) 22 component, (c) 33 component (d) 12 shearing component, at the end of loading of Vickers indentation (5 N) of an oxidized steel sample (thickness of oxide: 26 µm).

4. Discussion

4.1. Cracking/delamination mechanism

Combination of simulation and FIB analysis confirmed localization of circular and radial cracks reported in literature during the loading of indentation on thin films [21,26,31–34]. For delamination, shearing component is increasing all along the loading and is at the initiation of this phenomenon. It is in agreement with Rosenfeld model in which interfacial crack grows only during loading [12]. This mechanism differs from lateral cracks reported by Marshall [35] which propagated at the end of the unloading in bulk brittle material parallelly to the surface. In reality, degradation at the interface is in a mixed mode between I and II according to Rosenfeld [12]. The relative amount of each mode can be described by the phase angle $\tan\alpha = K_{II}/K_I$ (0° for a pure crack opening and 90° for a pure shear loading). For indentation of an epoxy-glass interface, the authors found $\alpha = 45°$ to 55°. The influence of fracture mode on G_c has been widely described in literature ; by increasing α, G_c tends to increase too, an explanation is crack tip plasticity and non-planar interface [12]. In this model, buckling and residual stress are not accounted for, and hardness is supposed to be constant through thickness. Compressive stress strongly influenced delamination by increasing driving force of interfacial cracks when buckling occurs [11]. A limitation in the application of the model is that the FIB-milled zone must be larger than the delaminated area (Figure 6) (for technical issues, no cross-section larger than 300 µm are prepared). Otherwise, delamination radius c may be underestimated and therefore, G_c overestimated, especially for N1 and HS grades.

4.2. Influence of alloying elements

A large difference in adhesion value is observed between IF and others grades (for a same oxidation cycle and preparation). In literature [36], alloying elements, such as Ni, modify ability to be descaled. The removability of scale is reduced due to the existence of a small amount of Ni. Thus, interface is uneven which reduces crack propagation. In our tests, there are differences of Mn and C percentage. It could explain difference in the adhesion values calculated. Effects of these alloying elements are discussed by Kizu [37]. In his study, specimens are oxidized at high temperature and blistering is observed. Scale blistering is the balance between delaminating (by compressive buckling or gas formation at the interface) and adhesive forces between steel and oxide. For a fixed oxidation time, blistering tends to decrease for oxidation at T>800°, when the percentage of Mn is higher than 0.2. At 800°C, for %wC > 0.02, the same tendency is observed. Thus, high C and Mn content tends to promote blistering, and decrease adhesion of oxide. Several explanations are possible. At the interface, with more carbon, CO is more liable to be generated by selective oxidation of carbon, and adhesive force decreases. This tendency is also confirmed by Chandra-Ambhorn [38]: lower scale adhesion is related to the higher amount of carbon at the scale-steel interface, favouring CO gas or graphite formation. In addition, according to Kizu [37], wüstite, the main oxide phase, normally has a strong fiber texture {100}. The increasing percentage of Mn tends to favour other crystalline orientations such as {110} and {111}. The volume occupied by these two minority orientations causes compressive stress due to the different crystal growth rates. It deteriorates adhesion between oxide and substrate. Mn also affects the grain size of wüstite. With a lower grain size, others crystalline orientations {110} and {111} are more present, which increases compressive stress.

4.3. Oxide adhesion in literature

In the literature, other methods are used to determine adhesion of oxide at room temperature (Table 4): tensile tests [38–41], inverted blister-test [42], scratch test [43] and indentation [44,45]. Large variability is also observed in adhesion values. It confirms difficulty to characterize adhesion of thin oxide steel. Ahtoy [44] used RT Vickers indentation to study the interface of low carbon oxidized steel as an utilization of the method described by Drory and Hutchinson [10]. Her study mainly focused on alloying elements such as P, Al and Si. For a P-containing steel oxidized at 1000°C, adhesion energy lies in the range of 0 – 350 J/m^2, which means that certain areas are initially non-adherent while interface is tough at other places. Oxide adhesion was also calculated by Chandra-Ambhorn et al. using tensile test [39] by considering that spallation of oxide occurs when energy stored in oxide exceeds energy required to separate scale-metal interface. During the test, spallation ratio (spalled area divided by total area of sample) was calculated using quantitative image analysis. Their conclusion was that adhesion is influenced by residual stresses (an initially stored energy) and Young's modulus (to which elastic strain energy is proportional). Indeed, higher Young's modulus gave higher quantified mechanical adhesion energy. In our experiments, oxide is composed of three phases, which have different properties. SEM observations show different proportions of phases for N1 and HS (Figure 6) for which magnetite is the main phase and has a higher Young modulus than wüstite [46]. This variation fosters heterogeneity in adhesion values calculated. Similarly, Nilsonthi et al. [47] used macro-tensile tests, in order to evaluate adhesion of steel oxide (mainly magnetite); they found that Si tends to increase adhesion by precipitation of SiO_2 at the interface between steel and iron oxides. Another study highlights influence of temperature and humidity [40]. High temperature at the end of the finishing mill tends to decrease adhesion, by increasing diffusion rate which creates defects at the interface. Adhesion further decreases after oxidation in humidified atmosphere. Inverted blister test was used to quantify adhesion of thermal oxide layers (1 µm) grown on ferritic stainless steel (18% Cr) [42]. Alloying elements, such as Ti and Nb, have a great influence on adhesion values calculated. TiO_2 precipitates at the interface anchor the oxide layer but intermetallic precipitates (Fe_2Nb) are harmful for adhesion. Macro-scratch test is used by Noh [43] to estimate spallation of oxide which occurs during uncoiling of low carbon steel. A combined experimental and simulation method is carried out to determine the value of fracture energy, it is estimated to 18 J/m^2 (thickness < 30 µm).

1.1. It can be concluded that variability is inherent to the adhesion of oxides on steels and that, even if conditions of oxidation are specific to each case, our RT indentation oxide adhesion tests are in agreement with literature. In an industrial context, N1 and HS grades are difficult to descale. It is known that the descaled slab surface shows alternance of well-descaled areas and remaining fragments of oxide. During the process, if oxide has a large heterogeneity in adhesion values such as shown by the present measurements, it may induce such a composite area where when local oxide is not well delaminated. In the roll bite, this remaining oxide fragments will be embedded in steel and may disturb re-oxidation. At the end of the finishing mill, surface defects are more liable to be present. The uncertainty exposed in 1.2.

Table ***2*** therefore does not plead against indentation but reveals heterogeneity of interface properties strongly linked with poor descalability.

Table 4. Comparison of the quantified mechanical adhesion energies of the oxide scale on metallic substrates using different methods.

Material	Oxidising conditions	Adhesion energy (J/m^2)	Method used	Reference
Low carbon steel	650-700° up to 10 minutes (15 to 55μm)	0-474	Indentation test	This work
Low carbon steel (0,04%)	Finishing mill temperature from 820 to 910°C	44-890	Tensile test	[40]
Low carbon steel (0,16%C)	850 °C in O2–20H2O up to 120 s	18-240	Tensile test	[39]
Low carbon steel	As-received steels from hot rolling process (recycled and conventional steel)	2-690	Tensile test	[47]
P-containing steel	1000 °C in laboratory air up to 10 min	0-350	Indentation test	[44]
Ferritic Stainless Steel	900°C in Ar–15O2 to obtain the scale thickness of about 2 μm	3-170	Inverted-blister test	[42]
Low carbon steel	900 °C (10 to 30μm)	18	Scratch Test	[43]

5. Conclusion and perspectives

The core of the project consists in designing and carrying out experiments at high temperature to understand the behaviour of scale and determine a stress-based fracture criterion relevant for the computation of descaling. At room temperature, adhesion has been successfully measured by indentation, highlighting the strong influence of alloying elements on the adhesion of oxide scale, particularly C and Mn. Adhesion values calculated agree with other studies. New grades, which are difficult to descale, are planned to be tested. Numerical simulation has confirmed the mechanism of cracking in surface (radial and circular) and delamination of oxide at the interface, by shear (mode II). Others methods to evaluate properties of oxide should be implemented to confirm these results. In simulations, Cohesive Zone model (CZM) will be implemented to allow cracking and delamination of oxide. Residual stresses (measured by X-Ray Diffraction) will be considered. In future work, similar instrumented indentation tests will be done at high temperature to evaluate the ductile-brittle transition of the oxide layer, and to quantify properties of the oxide. These tests will allow us to quantify influence of temperature on degradation mechanisms (crack, delamination...) in order to have a better understanding of the descaling process and allow numerical simulation of this process.

References

[1] PICQUÉ B 2004 *Experimental study and numerical simulation of iron oxide scales mechanical behavior in hot rolling* (PhD Dissertation, ENSMP)
[2] Suárez L, Houbaert Y, Eynde X V and Colás R 2009 High temperature deformation of oxide scale *Corrosion Science* **51** 309–15

[3] Filatov D, Pawelski O and Rasp W 2004 Hot-rolling experiments on deformation behaviour of oxide scale *Steel Research International* **75** 20–5
[4] Krzyzanowski M and Beynon J H 2006 Modelling the behaviour of oxide scale in hot rolling *ISIJ International* **46** 1533–47
[5] Berns H, Fischer A and Kleff J 1993 Scratch tests on iron-, nickel- and cobalt-based alloys at elevated temperatures *Wear* **162–164** 585–9
[6] Varga M, Leroch S, Rojacz H and Ripoll M R 2017 Study of wear mechanisms at high temperature scratch testing *Wear* **388–389** 112–8
[7] Allsopp D N and Hutchings I M 2001 Micro-scale abrasion and scratch response of PVD coatings at elevated temperatures *Wear* **251** 1308–14
[8] Pujante J, Vilaseca M, Casellas D and Riera M D 2014 High temperature scratch testing of hard PVD coatings deposited on surface treated tool steel *Surface and Coatings Technology* **254** 352–7
[9] Beake B D, Endrino J L, Kimpton C, Fox-Rabinovich G S and Veldhuis S C 2017 Elevated temperature repetitive micro-scratch testing of AlCrN, TiAlN and AlTiN PVD coatings *International Journal of Refractory Metals and Hard Materials* **69** 215–26
[10] Drory M D and Hutchinson J W 1996 Measurement of the adhesion of a brittle film on a ductile substrate by indentation *Proceedings of the Royal Society of London. Series A: Mathematical, Physical and Engineering Sciences* **452** 2319–41
[11] Marshall D B and Evans A G 1984 Measurement of adherence of residually stressed thin films by indentation. I. Mechanics of interface delamination *Journal of Applied Physics* **56** 2632–8
[12] Rosenfeld L G, Ritter J E, Lardner T J and Lin M R 1990 Use of the microindentation technique for determining interfacial fracture energy *Journal of Applied Physics* **67** 3291–6
[13] Vlassak J J, Drory M D and Nix W D 1997 A simple technique for measuring the adhesion of brittle films to ductile substrates with application to diamond-coated titanium *Journal of Materials Research* **12** 1900–10
[14] Kriese M D, Gerberich W W and Moody N R 1999 Quantitative adhesion measures of multilayer films: Part I. Indentation mechanics *Journal of Materials Research* **14** 3007–18
[15] Kriese M D, Gerberich W W and Moody N R 1999 Quantitative adhesion measures of multilayer films: Part II. Indentation of W/Cu, W/W, Cr/W *Journal of Materials Research* **14** 3019–26
[16] Vasinonta A and Beuth J L 2001 Measurement of interfacial toughness in thermal barrier coating systems by indentation *Engineering Fracture Mechanics* **68** 843–60
[17] Wheeler J M, Oliver R A and Clyne T W 2010 AFM observation of diamond indenters after oxidation at elevated temperatures *Diamond and Related Materials* **19** 1348–53
[18] Tiphéne G, Baral P, Comby-Dassonneville S, Guillonneau G, Kermouche G, Bergheau J-M, Oliver W and Loubet J-L 2021 High-temperature scanning indentation: A new method to investigate in situ metallurgical evolution along temperature ramps *Journal of Materials Research* **36** 2383-96
[19] Amano T, Okazaki M, Takezawa Y, Shiino A, Takeda M, Onishi T, Seto K, Ohkubo A and Shishido T 2006 Hardness of oxide scales on Fe-Si alloys at room- and high-temperatures *Materials Science Forum* **522–523** 469–76
[20] Bredl J, Dany M, Schneider H-C and Kraft O 2016 Instrumented indentation at elevated temperatures for determination of material properties of fusion relevant materials *Nuclear Materials and Energy* **9** 502–7
[21] Xiao Y, Shi W, Wan Q and Luo J 2019 Evaluation of failure properties of a DLC/steel system using combined nanoindentation and finite element approach *Diamond and Related Materials* **93** 159–67
[22] Abdul-Baqi A and Van der Giessen E 2002 Numerical analysis of indentation-induced cracking of brittle coatings on ductile substrates *International Journal of Solids and Structures* **39** 1427–42
[23] Xiao Y, Shi W and Luo J 2015 Indentation for evaluating cracking and delamination of thin coatings using finite element analysis *Vacuum* **122** 17–30
[24] Xu X-P and Needleman A 1994 Numerical simulations of fast crack growth in brittle solids *Journal of the Mechanics and Physics of Solids* **42** 1397–434

[25] Lee J H, Gao Y F, Johanns K E and Pharr G M 2012 Cohesive interface simulations of indentation cracking as a fracture toughness measurement method for brittle materials *Acta Materialia* **60** 5448–67
[26] Weppelmann E and Swain M V 1996 Investigation of the stresses and stress intensity factors responsible for fracture of thin protective films during ultra-micro indentation tests with spherical indenters *Thin Solid Films* **286** 111–21
[27] AFNOR 2018 ISO 6507-1:2005 (standard)- Essai de dureté Vickers (Vickers Hardness Test)
[28] Krzyzanowski M and Beynon J H 1999 Finite element model of steel oxide failure during tensile testing under hot rolling conditions *Materials Science and Technology* **15** 1191–8
[29] Tabor D 1951 *The Hardness of Metals* (OUP Oxford)
[30] Huntz A M and Schütze M 1994 Stresses generated during oxidation sequences and high temperature fracture *Materials at High Temperatures* **12** 151–61
[31] Chai H and Lawn B R 2004 Fracture mode transitions in brittle coatings on compliant substrates as a function of thickness *Journal of Materials Research* **19** 1752–61
[32] Pachler T, Souza R M and Tschiptschin A P 2007 Finite element analysis of peak stresses developed during indentation of ceramic coated steels *Surface and Coatings Technology* **202** 1098–102
[33] Fu K, Yin Y, Chang L, Shou D, Zheng B and Ye L 2013 Analysis on multiple ring-like cracks in thin amorphous carbon film on soft substrate under nanoindentation *J. Phys. D: Appl. Phys.* **46** 505314
[34] Hainsworth S V, McGurk M and Page T 1998 The effect of coating cracking on the indentation response of thin hard-coated systems *Surface and Coating Technology* **102** 97-107
[35] Marshall D B, Lawn B R and Evans A G 1982 Elastic/plastic indentation damage in ceramics: the lateral crack system *Journal of the American Ceramic Society* **65** 561–6
[36] Asai T, Soshiroda T and Miyahara M 1997 Influence of Ni impurity in steel on the removability of primary scale in hydraulic descaling *ISIJ International* **37** 272–7
[37] Kizu T, Nagataki Y, Inazumi T and Hosoya Y 2001 Effects of chemical composition and oxidation temperature on the adhesion of scale in plain carbon steels *ISIJ International* **41** 1494–501
[38] Chandra-ambhorn S, Phadungwong T and Sirivedin K 2017 Effects of carbon and coiling temperature on the adhesion of thermal oxide scales to hot-rolled carbon steels *Corrosion Science* **115** 30–40
[39] Chandra-ambhorn S and Klubvihok N 2016 Quantification of adherence of thermal oxide scale on low carbon steel using tensile test *Oxid Met* **85** 103–25
[40] Chandra-ambhorn S, Ngamkham K and Jiratthanakul N 2013 Effects of process parameters on mechanical adhesion of thermal oxide scales on hot-rolled low carbon steels *Oxid Met* **80** 61–72
[41] Na Kalasin N, Yenchum S and Nilsonthi T 2018 Adhesion behaviour of scales on hot-rolled steel strips produced from continuous casting slabs *Materials Today: Proceedings* **5** 9359–67
[42] Mougin J, Le Bihan T and Lucazeau G 2001 High-pressure study of Cr2O3 obtained by high-temperature oxidation by X-ray diffraction and Raman spectroscopy *Journal of Physics and Chemistry of Solids* **62** 553–63
[43] Noh W, Lee J-M, Kim D-J, Song J-H and Lee M-G 2019 Effects of the residual stress, interfacial roughness and scale thickness on the spallation of oxide scale grown on hot rolled steel sheet *Materials Science and Engineering: A* **739** 301–16
[44] Ahtoy E 2010 *Effect of alloying elements (Si, Al, P, B) on low carbon steel oxidation in low process at high temperatures : mechanisms and modelling.* (PhD Dissertation, University of Grenoble-Alpes)
[45] Monteiro M J, Saunders S R J and Rizzo F C 2011 The effect of water vapour on the oxidation of high speed steel, kinetics and scale adhesion *Oxid Met* **75** 57–76
[46] Robertson J and Manning M I 1990 Limits to adherence of oxide scales *Materials Science and Technology* **6** 81–92
[47] Nilsonthi T, Chandra-ambhorn S, Wouters Y and Galerie A 2013 Adhesion of thermal oxide scales on hot-rolled conventional and recycled steels *Oxid Met* **79** 325–35

Acknowledgement
The authors thank the French National Agency for Technological Research (ANRT), for the PhD grant of VCB, CIFRE #2019/1210.